

Review

Use of Silicon Photomultipliers in the Detectors of the JEM-EUSO Program

Francesca Bisconti  on behalf of the JEM-EUSO Collaboration

Istituto Nazionale di Fisica Nucleare—Sezione di Roma Tor Vergata, Via della Ricerca Scientifica 1, 00133 Rome, Italy; francesca.bisconti@roma2.infn.it

Abstract: The JEM-EUSO program aims to study ultra-high energy cosmic rays from space. To achieve this goal, it has realized a series of experiments installed on the ground (EUSO-TA), various on stratospheric balloons (with the most recent one EUSO-SPB2), and inside the International Space Station (Mini-EUSO), in light of future missions such as K-EUSO and POEMMA. At nighttime, these instruments aim to monitor the Earth's atmosphere measuring fluorescence and Cherenkov light produced by extensive air showers generated both by very high-energy cosmic rays from outside the atmosphere and by neutrino decays. As the two light components differ in duration (order of microseconds for fluorescence light and a few nanoseconds for Cherenkov light) they each require specialized sensors and acquisition electronics. So far, the sensors used for the fluorescence camera are the Multi-Anode Photomultiplier Tubes (MAPMTs), while for the Cherenkov one, new systems based on Silicon PhotoMultipliers (SiPMs) have been developed. In this contribution, a brief review of the experiments is followed by a discussion of the tests performed on the optical sensors. Particular attention is paid to the development, test, and calibration conducted on SiPMs, also in view to optimize the geometry, mass, and weight in light of the installation of mass-critical applications such as balloon- and space-borne instrumentation.

Keywords: JEM-EUSO; SiPM; cosmic rays; extensive air-showers; fluorescence detector; Cherenkov detector; space instruments



Citation: Bisconti, F., on behalf of JEM-EUSO Collaboration. Use of Silicon Photomultipliers in the Detectors of the JEM-EUSO Program. *Instruments* **2023**, *7*, 55. <https://doi.org/10.3390/instruments7040055>

Academic Editor: Antonio Ereditato

Received: 12 October 2023

Revised: 24 November 2023

Accepted: 24 November 2023

Published: 14 December 2023



Copyright: © 2023 by the author. Licensee MDPI, Basel, Switzerland. This article is an open access article distributed under the terms and conditions of the Creative Commons Attribution (CC BY) license (<https://creativecommons.org/licenses/by/4.0/>).

1. Introduction

In the last years, different types of semiconductor radiation detectors have been developed for fundamental science experiments. Silicon Photomultipliers (SiPMs) represent a novel category of photodetectors [1–3], with single photon detection capability and detection efficiencies reaching up to red $\sim 60\%$ (at peak wavelength of ~ 450 nm) under normal operating conditions, and achieving single-photon time resolutions in the range of red tens to hundreds of picoseconds, red depending on the channel size [4]. Thanks to significant advancements in SiPM technology in recent years, these detectors can be closely compared to traditional PhotoMultiplier Tubes (PMTs), which have long been dominant in the realm of photon detection. SiPMs offer numerous advantages, such as significantly lower operating voltage, a lightweight and durable structure, and immunity to magnetic fields [5]. They exhibit robustness against excessive incident light; instead of damaging the collecting anode as in a PMT, a SiPM saturates, drawing constant current without harm. Nevertheless, SiPM characteristics are strongly influenced by temperature [6].

The Joint Exploratory Missions for an Extreme Universe Space Observatory (JEM-EUSO) Program [7] consists of a series of telescopes and experiments operated on the ground (EUSO-TA [8]), on stratospheric balloons (EUSO-Balloon [9], EUSO-SPB1 [10], and EUSO-SPB2 [11]), and in the space inside the International Space Station (ISS-Mini-EUSO [12]). They all contribute in growing the knowledge and extending the capability to develop the technology to detect Ultra-High Energy Cosmic Rays (UHECRs) from space (aboard orbiting satellites) by observing the fluorescence and Cherenkov light emitted

during their path through the Earth's atmosphere and the Cherenkov emission from Earth skimming neutrinos. Such a future space-based experiment is the Probe of Extreme Multi-Messenger Astrophysics (POEMMA) Observatory [13], which will allow for the detection of Earth-skimming neutrinos and UHECRs via stereo measurements by two co-orbital telescopes with tilting capability in order to extend the observation area.

The use of Multi-Anode Photo-Multiplier Tubes (MAPMTs) in the indirect detection of UHECR via the observation of fluorescence and Cherenkov light is well established, as the focal surfaces of the JEM-EUSO fluorescence telescopes are made of MAPMTs. In Figure 1 the so-called Photon-Detection Module (PDM) with the focal surface made of MAPMTs (model R11265-M64 [14], $2.62 \times 2.62 \text{ cm}^2$, with $2.88 \times 2.88 \text{ mm}^2$ pixels) is visible on the left ($\sim 17 \times 17 \text{ cm}^2$ in total), while on the right two MAPMTs of the same model are represented together with an example of SiPM array (model S12642-0808PA-50 [15], $2.58 \times 2.58 \text{ cm}^2$, with $3 \times 3 \text{ mm}^2$ pixels), with similar size and same number of channels.

The PDM is the basic module of the focal surface of the detectors of the JEM-EUSO program. EUSO-TA, EUSO-Balloon, and EUSO-SPB1 and Mini-EUSO host one PDM, while EUSO-SPB3 hosted three PDMs. POEMMA is foreseen to host several tens of PDMs. One PDM is composed of 3×3 Elementary Cells (ECs), each one made of 2×2 MAPMTs. Each MAPMT is covered with a BG3 filter [16] to limit its sensitivity to the UV region (290–430 nm) and reduce the background of photons outside this optimal frequency band.

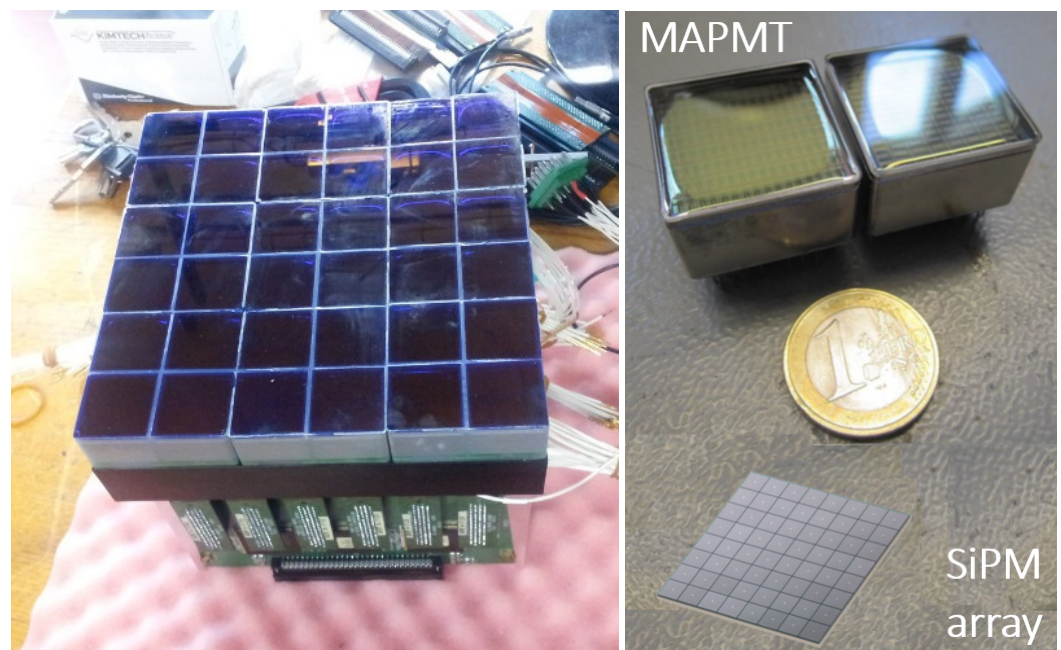


Figure 1. A PDM with the focal surface made of 36 MAPMTs (left), image taken from [17]; 2 MAPMTs and a SiPM array of similar size and number of channels (right), composition of images taken from [18] (MAPMTs) and adapted from Hamamatsu product information [15] (SiPM array).

The time resolution of most of the detectors of the JEM-EUSO program is $2.5 \mu\text{s}$, which was defined for the observations from space and kept also for the ground-based EUSO-TA and the first balloon-based EUSO-Balloon and EUSO-SPB1, in order to test the original design of a future space-based detector. It was reduced to $1 \mu\text{s}$ for the most recent balloon-based experiment EUSO-SPB2, to operate a mission with a more appropriate time resolution for observations from the stratosphere. These time lengths are called within the JEM-EUSO Collaboration Gate Time Units (GTUs).

Terrestrial detectors with SiPM have been developed in several experiments, such as the Cherenkov Telescope Array (CTA) [19], the First Auger Multi-pixel photon counter camera for the Observation of Ultra-high-energy air Showers (FAMOUS) [20], IceTop-Gen2 Scintillator Upgrade [21], etc.

The evaluation of SiPMs for non-terrestrial UHECR telescopes was performed and is still under study within the JEM-EUSO Collaboration. Several telescopes host additional cameras based on SiPMs to study the performance. In this contribution, these detectors will be described, paying particular attention to the SiPM cameras.

2. Detection of UHECRs and Skimming Neutrinos via the Fluorescence Technique

Cosmic rays are extraterrestrial particles, of which about 90% are hydrogen nuclei (protons), 9% are helium nuclei, and the remaining 1% is composed of heavier nuclei and electrons. Their energy range is from about 10^9 to 10^{20} eV or more. Over this energy range, the cosmic ray flux varies by many orders of magnitude, between $1 \text{ particle m}^{-2} \text{ s}^{-1}$ at low energies ($E \sim 10^9$ eV), $1 \text{ particle m}^{-2} \text{ yr}^{-1}$ at intermediate energies ($E \sim 10^{15}$ eV), $1 \text{ particle km}^{-2} \text{ yr}^{-1}$ at high energies ($E \sim 10^{19}$ eV), and $1 \text{ particle km}^{-2}$ per century at extreme energies ($E \sim 10^{20}$ eV).

Up to 10^{15} eV cosmic rays can be observed directly with detectors mounted on balloons or space-based experiments. At higher energies, the flux of particles is so low that huge detectors would be necessary to measure them directly. Therefore, indirect detection methods have been developed, observing the secondary cosmic rays, i.e., particles produced by the interaction of primary cosmic rays with the atmospheric molecules and originating the so-called Extensive Air Showers (EASs). Above 5×10^{19} eV, a strong suppression in the flux is observed, consistent with the Greisen–Zatsepin–Kuzmin (GZK) cutoff [22,23] that considers the interaction of protons with photons from the Cosmic Microwave Background (CMB), and with the photo-disintegration of nuclei. The origin of the suppression is, however, still debated and subject of studies. Moreover, protons in this energy range could directly point back to their sources, since their deflection due to magnetic fields would be small and would give indications about their origin.

Other astrophysical observable of interest are neutrinos. The Earth can be used as a large volume to let neutrinos interact and produce particles that, in turn, would decay and generate upward-going EASs with an upward-going Cherenkov cone that could be observed from above, with balloon- and space-based telescopes.

The main goals of the JEM-EUSO program are the detection of trans-GZK cosmic rays with high statistics, the study of their arrival directions and the anisotropy, the identification and study of the sources, and the detection of the Earth-skimming neutrinos. Building a large-scale detector observing the Earth's atmosphere from an orbiting satellite, provides the advantage of observing large areas of the atmosphere at one time, increasing the exposure of the detector for the observation of UHECRs. Moreover, orbiting around the Earth would provide a uniform coverage of the sky.

The detectors of the JEM-EUSO program use an indirect method to observe UHECRs and skimming neutrinos by measuring the fluorescence and Cherenkov light along the development of EASs in the atmosphere. This kind of telescope can only be operated at night-time, with good weather conditions, and in places with low artificial light background. A duty cycle of about 10–15% is expected for ground-based fluorescence detectors, intended as the fraction of time in which UHECRs can be observed, which is limited mainly by sunlight but also by the presence of other steady backgrounds like night-glow and moonlight. The fluorescence light is emitted by the relaxation of nitrogen molecules that have been excited by the interaction with charged particles in the EASs, mainly electrons and positrons. The fluorescence spectrum has lines in the UV band at discrete wavelengths in the range from 290 nm to 430 nm, with the most intense emission at around 337.1 nm [24]. The overall fluorescence emission along the shower development is isotropic. The Cherenkov light is produced when charged particles move through a medium with a velocity that is higher than the velocity of light in that medium. The particle ionizes the medium through its path, leaving a locally excited path behind. The following relaxation causes the emission of Cherenkov light within a cone that has an opening angle usually within $\sim 1.4^\circ$ and varying with the refractive index of the medium and the speed of

the particle. The emission spectrum of Cherenkov radiation is continuous and the photon yield is higher in the UV than in the visible band.

3. SiPMs in the JEM-EUSO Experiments

3.1. Brief Description of the SiPMs and Comparison with MAPMTs

A SiPM is composed of a matrix of identical microcells, each one consisting of a so-called Geiger-mode Avalanche Photodiode (G-APD) or Single-Photon Avalanche Diodes (SPAD) and a quenching resistor connected in series [1–3]. The microcells are connected in parallel to a bias voltage. SiPMs are also known as Multi-Pixel Photon Counters (MPPCs), naming a microcell as pixel. The pixel of a SiPM should not be confused with the pixel of a MAPMT: in a MAPMT every output channel gets the signal from one pixel; in a SiPM there can be several hundreds or even thousands of pixels per output channel. Every pixel produces the same signal when it is hit by a photon and the sum of the pixel responses gives the channel output. The typical dimension of a SiPM sensor is between $1 \times 1 \text{ mm}^2$ and $6 \times 6 \text{ mm}^2$ and the number of microcells per device ranges from several hundreds to several tens of thousands. Microcells vary between $10 \times 10 \text{ }\mu\text{m}^2$ and $100 \times 100 \text{ }\mu\text{m}^2$ in size (as examples: Onsemi MICROFC-10010-SMT with channel of $1 \times 1 \text{ mm}^2$ and microcell of $10 \times 10 \text{ }\mu\text{m}^2$, and MICROFC-60035-SMT with channel of $6 \times 6 \text{ mm}^2$ and microcell of $35 \times 35 \text{ }\mu\text{m}^2$ [25]; Hamamatsu S13360-1325CS with channel of $1.3 \times 1.3 \text{ mm}^2$ and microcell of $25 \times 25 \text{ }\mu\text{m}^2$, and S13360-6075CS with channel of $6 \times 6 \text{ mm}^2$ and microcell of $75 \times 75 \text{ }\mu\text{m}^2$ [26]).

SiPMs present an opportunity for constructing modular detector surfaces due to their compact and lightweight design. They operate with low voltage and exhibit insensitivity to magnetic fields [5]. Noteworthy properties are a rapid response time (in the order of redtens to hundreds of picoseconds [4]), the ability for single photon detection, high photon detection efficiency, and resilience to light-induced damage. However, with their semi-conductive nature and clustered G-APDs, SiPMs suffer from significant noise sources: reddark-count rate (DCR), afterpulses, and crosstalk red [1–3]. G-APD performance depends on temperature, affecting breakdown voltage and quench resistor due to semiconductor band gap sensitivity. redDark-count rate, resulting from thermal effects, can be reduced by decreasing the temperature and the operating voltage: the latter lowers the potential for a thermally excited electron to initiate an avalanche, but would also decrease gain and PDE. Afterpulses, secondary peaks caused by trapped electrons in silicon defects, occur after the main signal, typically at 1 photoelectron level. Afterpulse probability increases with overvoltage and pixel size. redCrosstalk occurs when a photon is detected in one microcell and the avalanche pulse in this microcell can trigger (with a certain probability) avalanches in the neighboring microcells, creating two or three times the signal of a microcell in a SiPM, even though the original photon was only one. As crosstalk events coincide with the original photon-induced signal, they are indistinguishable, introducing the possibility of fake signals in multi-photoelectron signals.

To build large sensitive areas, SiPMs can be arranged in arrays. Furthermore, some models are available with the Through Silicon Via (TSV) technology. In single SiPMs the cathode is wired on the sides of the SiPM active surface and arrays of single SiPMs would have a large dead space between them. In the SiPM arrays TSV the cathode is etched through the silicon wafer in the middle of the SiPM, building an electrical interconnection from the surface to the back of the SiPM device. This allows to reduce the gaps between adjacent SiPM channels.

At the time of the preparation of the first relatively large-scale camera with SiPMs, two SiPM arrays were studied: the former model S12642-0808PA-50 with a top protective layer of epoxy resin [15] and the newer S13361-3050AS-08 with a top protective layer of silicone [27], both from Hamamatsu. The different top protective layer gives a different sensitivity of the SiPMs to the UV light with wavelengths lower than 320 nm, which causes a loss of photons in the case of epoxy resin. In Figure 2 the characteristic fluorescence spectrum of nitrogen molecules is shown in the wavelength range 295–430 nm.

The Photon Detection Efficiency (PDE) for a MAPMT prototype from 2009 (Hamamatsu R11265-00-M64 [14]), a SiPM array with epoxy resin, and a SiPM array with silicone are overlapped to the fluorescence spectrum and limited to its wavelength range.

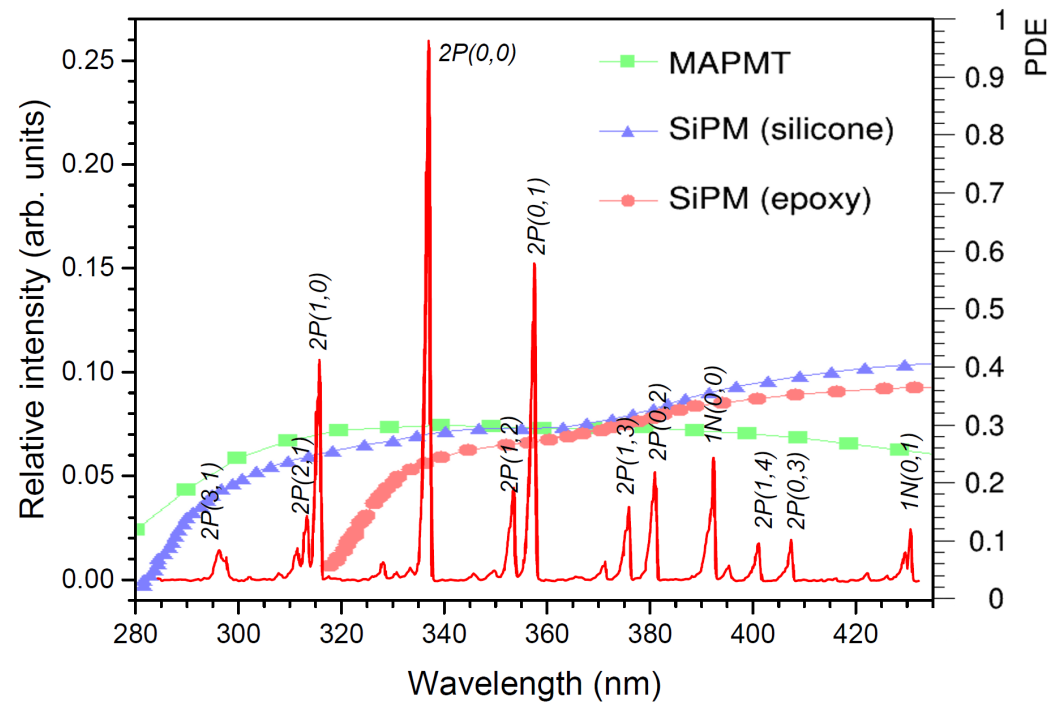


Figure 2. Fluorescence spectrum of nitrogen relaxation in the UV band from 280 nm to 435 nm at 800 hPa (about 2 km) measured by the AIRFLY Collaboration, taken from Ref. [24]. The area is scaled to unity. This shows that 25% of the spectrum intensity is due to the main line at 337.1 nm. PDEs of MAPMTs (calculated as the quantum efficiency present on the product datasheet and the collection efficiency of 80%, see the text) and SiPM arrays taken from Hamamatsu product information [14,15,27]. Image taken from Ref. [28].

The PDE for MAPMTs is defined as the quantum efficiency multiplied by the collection efficiency. The quantum efficiency of a MAPMT channel is the number of photoelectrons emitted by the photocathode divided by the number of incident photons; the collection efficiency is the probability that photoelectrons will land on the effective area of the first dynode of a MAPMT channel, assumed to be 80%. The PDE for SiPMs is the quantum efficiency multiplied by the fill factor and the avalanche triggering probability. In this case, the quantum efficiency is the number of electron-hole pairs generated by photons divided by the number of incident photons on the photosensitive area and the fill factor takes into account the dead area between one cell and the next one. In the plot it is visible that the SiPM with epoxy resin is not sensitive to the first three lines of the fluorescence spectrum, and MAPMTs and SiPM with silicone layer have a similar trend at the lower wavelengths up to about 380 nm, beyond which the SiPM array models become more efficient than MAPMTs. As anticipated, there are several differences in using SiPMs instead of MAPMTs, which include advantages and disadvantages and are indicated in Table 1.

Table 1. Differences between SiPMs and MAPMTs [29,30].

Characteristics	SiPMs	MAPMTs
Operation Voltage	~60 V (min. ~30 V [30])	~1000 V
Gain	10^5 – 10^7	10^5 – 10^7
PDE	20–60%	20–40%
Spectrum	300–900 nm (peak 450 nm)	300–650 nm (peak 340 nm)
DCR	$\sim 10^5$ cps/mm ²	$\sim 10^2$ cps/mm ²
Behaviour in magnetic fields	good	bad
Temperature insensitivity	no	yes
Robustness and compactness	yes	no

One main difference is the operation voltage, which is lower for SiPMs than MAPMTs. They are not sensitive to magnetic fields and resistant to bright conditions: they saturate without damage, while the anodes of PMTs get damaged. Moreover, they are compact and light. However, the thermal noise is an issue for SiPMs that must be mitigated by operating a cooling system to maintain the silicon junction at a lower temperature. The dark-count rate of SiPMs at room temperature is about three orders of magnitude higher than that of traditional PMTs. The production of SiPMs is automated, while MAPMTs are assembled by hand. This lets us foresee a reduction of the cost of SiPMs with time and area, making the construction of large telescopes financially feasible in addition to providing scientific advantages.

3.2. EUSO-SPB1 (SiECA)

The Extreme Universe Space Observatory on a Super Pressure Balloon (EUSO-SPB1—formerly simply called EUSO-SPB) [10] was the first experiment of the JEM-EUSO program that operated with a SiPM camera onboard. It was installed on a Super Pressure Balloon (SPB) developed by NASA for the 2017 campaign. It was launched on 24 April 2017 at 23:51 UTC from Wanaka, New Zealand, as a mission of opportunity on a NASA Super Pressure Balloon test flight planned to circle the southern hemisphere supported by a fast stratospheric air circulation that develops twice a year at about 33 km (7 mbar) above the southern ocean. This circulation flows easterly in the southern fall and westerly in the southern spring. SPBs are designed to float at a constant displacement volume and consequently, at a constant altitude for months, complete an orbit every few weeks and terminate on land.

The scientific goals were to make the first observations of UHECRs by looking down on the atmosphere with a UV fluorescence detector from the near space altitude of 33 km; and measure background UV light at night over ocean and clouds. Unfortunately, after 12 days 4 h, the flight was terminated prematurely in the Pacific Ocean, about 300 km SE of Easter Island, due to a leak in the balloon. Despite the setbacks, the EUSO-SPB1 instrument operated successfully while aloft and returned about 60 GB of data.

The EUSO-SPB1 optics was made of two 1 m² Poly(methyl methacrylate) (PMMA) plastic Fresnel lenses, which focus the light on a main focal surface made of a PDM, providing a field of view of $11.1^\circ \times 11.1^\circ$. The design of the detector is visible in Figure 3. The figure includes pictures for the telescope during the launch phase.

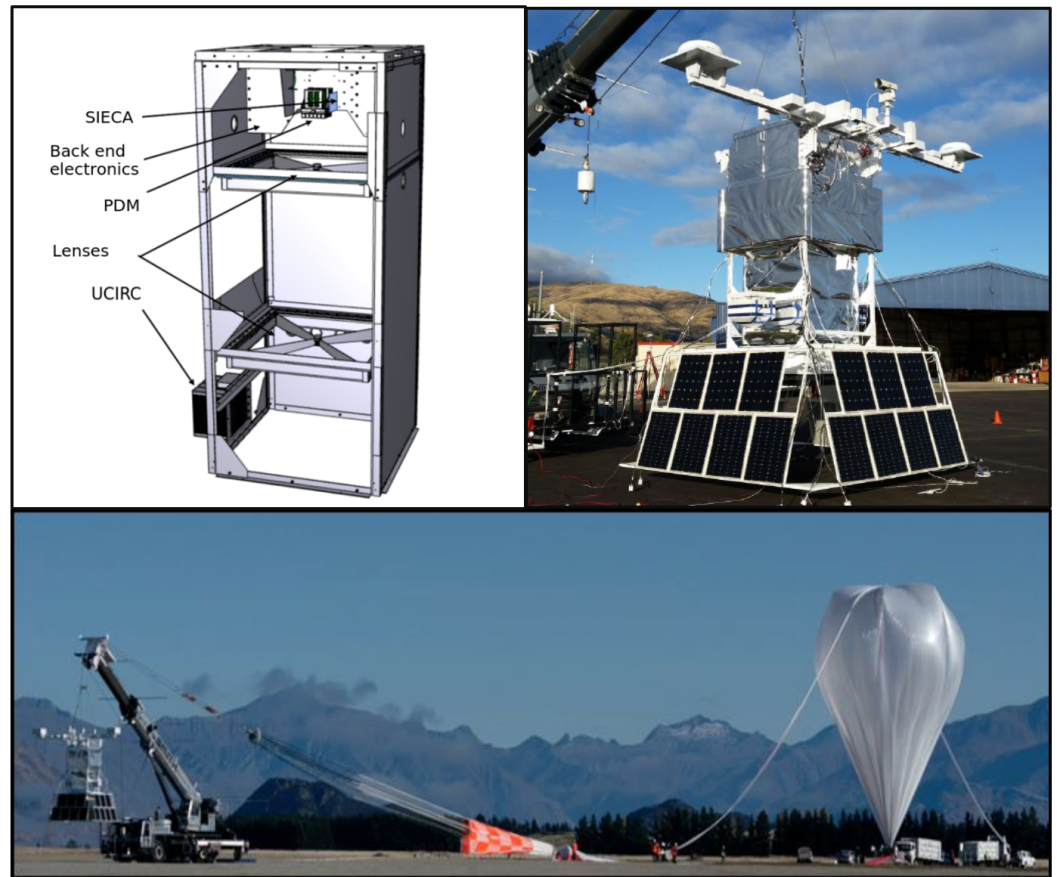


Figure 3. Images for the EUSO-SPB1 experiment. Sketch of the gondola with the PDM and an indication of the SiECA position (**top-left**). Pictures of EUSO-SPB1 before the launch (**top-right, bottom**). Images at the top taken from Ref. [31] and image at the bottom taken from Ref. [10].

An infrared (IR) camera system was developed and deployed to capture IR images of the area below EUSO-SPB1. The objective was to identify clouds and approximate the heights of cloud tops. The analysis of clouds is crucial for assessing the exposure of EUSO-SPB1, as high-altitude clouds diminish the available aperture of fluorescence telescopes operating at high altitudes [32]. The University of Chicago Infrared Camera (UCIRC) [33] was equipped with two identical IR cameras oriented toward the same region, featuring a field of view of $24^\circ \times 30^\circ$. Each camera was equipped with an IR filter. One filter transmitted IR light in the range 11.5–12.9 mm, while the other transmitted IR light in the range 9.6–11.6 mm. These specific ranges were chosen because they closely align with the typical black body peak for clouds. The methodology for measuring cloud color temperature, from which cloud top height can be derived, is elaborated in Ref. [34].

As an R&D test, the EUSO-SPB1 focal surface also included the Silicon Elementary Cell Add-on (SiECA) camera [35], with a 256 channel SiPM array that was mounted next to the PDM made of MAPMTs, on the same focal plane, and flown in a stand-alone sampling mode. This camera is described in more detail in the next section.

SiECA

The SiECA camera was built to test SiPMs as possible replacements for the MAPMTs used up to that time in the focal surface of telescopes of the JEM-EUSO program. The SiECA camera ($\sim 5 \times 5 \text{ cm}^2$, with $\sim 3 \times 3 \text{ mm}^2$ pixels) is visible in Figure 4 on the left side. On the right side of the same figure, it is installed next to the PDM ($\sim 17 \times 17 \text{ cm}^2$, with $\sim 2.88 \times 2.88 \text{ mm}^2$ pixels).

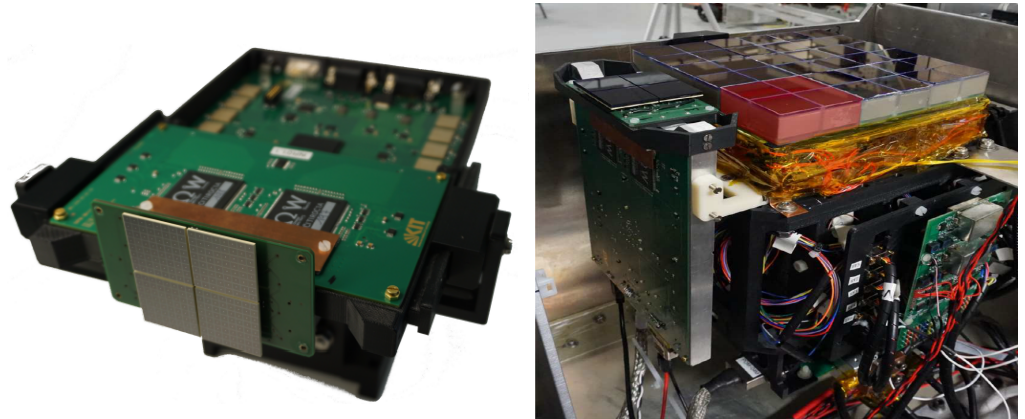


Figure 4. The SiECA camera (left); The SiECA camera assembled next to the EUSO-SPB1 PDM (with the noise-influenced EC of the PDM highlighted in red) (right). Images taken from Ref. [35].

Being placed next to the PDM, it would have allowed the observation of UHECR events with both the detectors. An example of a UHECR event simulated with the ESAF software [36] is visible in Figure 5 on the left, showing a proton event of energy 1.1×10^{19} eV and zenith angle 22.31° detected by both SiECA and the PDM. The signal was integrated over 41 GTUs, in order to have the track visible in a single frame. The panel on the right side of the same figure refers to a full camera test with a non-uniform light source, where the signal was integrated in 1 GTU. In both images, gaps between the MAPMTs of the PDM and between the SiPM arrays of SiECA are neglected.

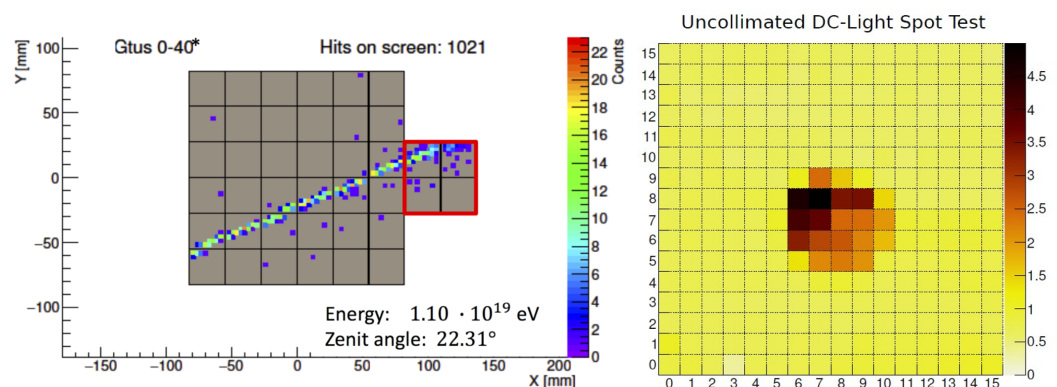


Figure 5. Simulation and measurement in the laboratory of the SiECA response. Simulation of a proton event of energy 1.1×10^{19} eV and zenith angle 22.31° detected by both SiECA and the PDM (left). The signal has been integrated over 41 GTUs and no background is added to the plot. Image taken from Ref. [37]. Full camera test with non-uniform light source. The response is the average photons detected per GTU (right). Image taken from Ref. [35]. Gaps between the MAPMTs of the PDM and between the SiPM arrays of SiECA are neglected in both images.

To make a full assessment of the currently available technology, hardware components were selected from available devices already on the market. Four 64-channel S13361-3050AS-08 SiPM arrays from Hamamatsu were arranged in a square of similar spacing to the EC of the JEM-EUSO PDMs. Details about the calibration of these sensors are available in Ref. [38]. The camera was biased by eight bias voltage generators (Hamamatsu C11204-02), and read out by eight Application Specific Integrated Circuit (ASIC) boards (Weeroc Citiroc 1A). The acquisition was controlled by a Field Programmable Gate Array (FPGA—Spartan6). Power was delivered by a commercial DC-DC converter to step down the available battery supply (26–32 V) to the required 5 V. Use of 3D printed mounting brace (off-white plastic between SiECA and PDM) provided thermal and electrical isolation.

Preliminary evaluation of the measurements made by SiECA during flight show that all channels of the camera are responding and sensitive to low-intensity light. Complications

during the flight due to a leakage from the SPB led to an unexpected trajectory, descending during night and rising during day. Moreover, due to electrical interference, seemingly from the SiECA camera, causing instability in the EC of the PDM highlighted in red in Figure 4 on the right, SiECA was often switched off during the flight. Figure 6 represents the trajectory of EUSO-SPB1, and green circles indicate the periods in which SiECA operated.

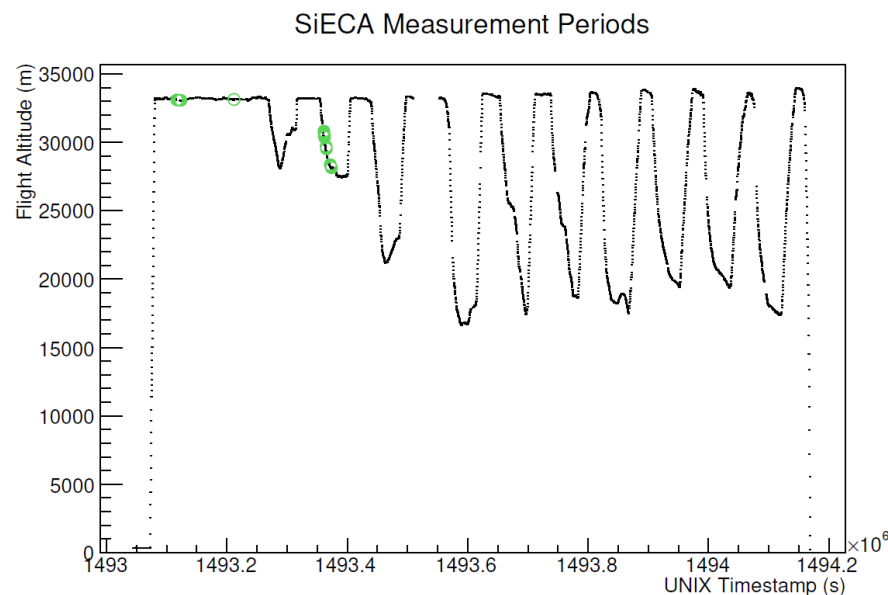


Figure 6. EUSO-SPB1 altitude with SiECA operation periods indicated in green circles. Descents indicate night cold cycles, then rising with the heat from the Sun. Image taken from Ref. [35].

During the short flight, SiECA collected nearly 400 events, mainly due to electronic noise, but none of them were related to UHECR events. However, the development of the SiECA camera and subsequent test flight on the EUSO-SPB1 mission has provided extensive information about the operation of SiPM at the low temperatures and pressures of the upper atmosphere. The SiECA camera was reproduced for further tests on ground [35].

3.3. EUSO-SPB2 (Cherenkov Telescope)

The Extreme Universe Space Observatory on a Super Pressure Balloon 2 (EUSO-SPB2) [11] is the successor experiment of EUSO-SPB1 and a pathfinder for the space-based mission POEMMA [13], a proposed dual satellite mission for the detection of UHECRs with energy above 1 EeV and very-high energy neutrinos, with energy above 1 PeV.

POEMMA will detect UHECRs via the fluorescence light emitted by EASs in the atmosphere. It will observe neutrinos by measuring the Cherenkov light emitted by EASs produced by the interaction or decay of charged leptons in the atmosphere after a neutrino propagates through the Earth and interacts near the surface. To perform both kinds of observations, each POEMMA telescope features a hybrid focal surface. As a pathfinder for POEMMA, EUSO-SPB2 was also designed to detect UHECRs and neutrinos, but with two different telescopes: a Fluorescence Telescope (FT) and a Cherenkov Telescope (CT), see Figure 7. The main goal for the FT was to observe UHECRs from above via the fluorescence technique for the first time, pointing directly downward. The CT was intended to measure cosmic rays with the direct Cherenkov technique for the first time, when pointed above the limb of the Earth, and to measure optical background for neutrino searches and search for astrophysical neutrinos when pointed below the limb.

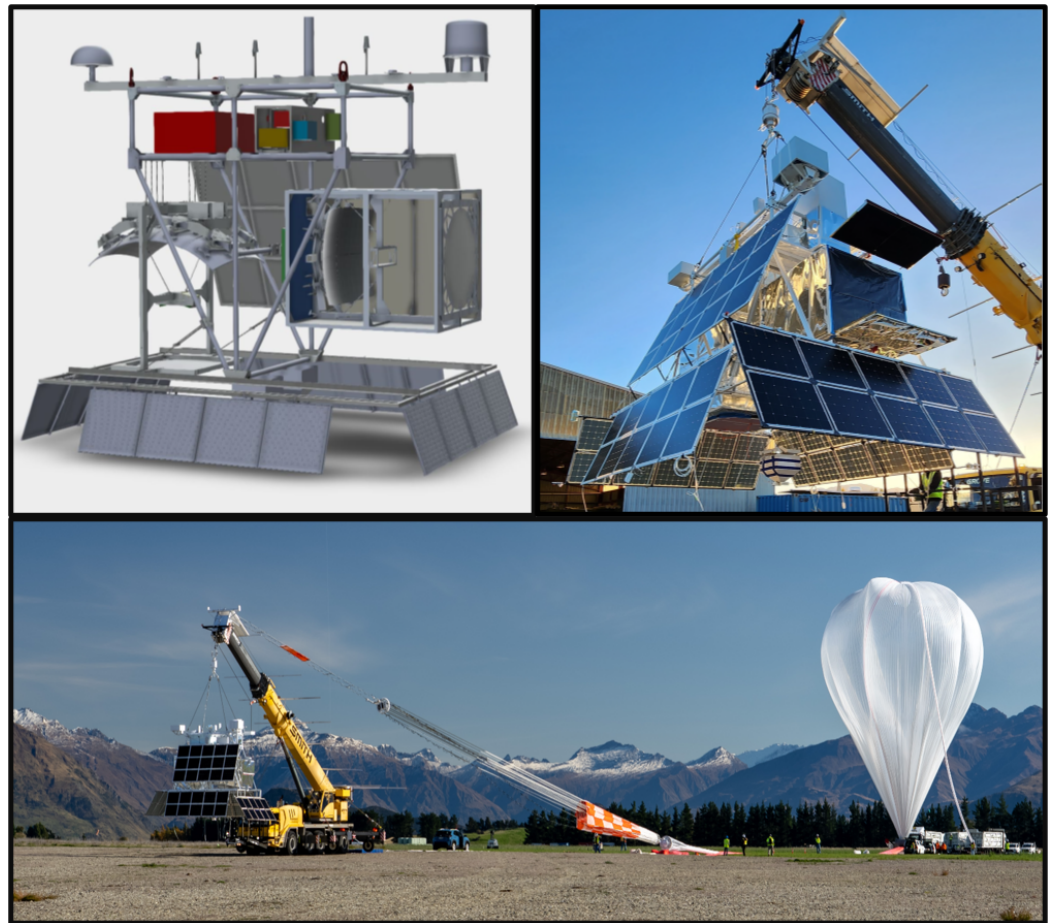


Figure 7. Images for the EUSO-SPB2 experiment. Sketch of the gondola with the fluorescence (left in the sketch) and the Cherenkov (right in the sketch) detectors (top-left). Pictures of EUSO-SPB2 before the launch (top-right, bottom). Images taken from Refs. [39–41].

The FT [42] was a 1 m diameter modified Schmidt telescope, focusing the light on three PDMs with MAPMTs (Hamamatsu R11265-M64-203 [14]) read out by ASIC boards (SPACIROC3) [43] that allowed a double pulse resolution of 6 ns and an integration time of 1 μ s. The trigger [44] operated individually on each PDM. The field of view was $36^\circ \times 12^\circ$ with a fixed nadir pointing direction. A central data processor [45] connected the three PDMs and enabled a synchronized readout if one PDM was triggered. More information about the performance and the calibration of the FT is available in Refs. [39,42].

The CT [41] was a 1 m diameter modified Schmidt telescope featuring a bifocal alignment of four mirror segments and an elongated camera constructed with SiPM arrays designed for observing the Earth's limb. A more in-depth discussion of this telescope is provided in the next section, and additional information can be referenced in Refs. [41,46].

Additionally, the EUSO-SPB2 mission terminated prematurely, concluding after merely 1 day, 12 h, and 53 min, in the Pacific Ocean. This premature termination was attributed to a balloon leak. Nevertheless, the collected data indicates that all instruments were successfully activated at the floating altitude and operated effectively throughout the duration of the flight.

Cherenkov Telescope of EUSO-SPB2

The CT [41] optics is based on a Schmidt catadioptric system, with a 1 m² light collection area segmented into four identical mirrors, and with a focal length of 860 mm. A corrector lens at the entrance of the telescope controls aberrations. The effective aperture area is reduced to 0.785 m² taking into account the shadowing from the camera, transmission losses from the corrector plate, and reflection/scattering losses at the mirror. A

particularity of the telescope is its bi-focal optics, achieved by rotating the optical axis of the lower and upper row of mirrors 0.4° relative to each other [47]. The bi-focal optics projects the image twice on the camera with a horizontal offset of 12 mm. This allows the discrimination between signals from noise or cosmic rays that interact directly with the instrument and that leave only one image, and the signals coming from outside the detector that, reflected by the bi-focal optics, produce a double image.

The camera focal plane is curved with a radius of 850 mm, see Figure 8. It hosts 8×4 SiPM arrays (Hamamatsu S14521-6050AN-04 [48]) in the horizontal and vertical, 4×4 channels ($6.4 \times 6.4 \text{ mm}^2$ each), for a total of 512 channels. With respect to other SiPM array models with smaller pixels (e.g., the one used for SiECA) the size of a single pixel in the CT worsens the spatial resolution. However, having fewer pixels in the telescope reduced the power consumption required by the read-out electronics. The used SiPM array has a broad wavelength sensitivity in the range 200–1000 nm, with a peak PDE of 50% at 450 nm. The wide spectral response reaches into the IR, which is ideal for our purpose, because, due to absorption and scattering effects, only the red components of the Cherenkov light arrive at the telescope from far-away showers, such as the ones expected from Earth-skimming neutrinos. At the operating voltage, direct optical crosstalk is only 1.5% and the temperature dependence of the gain is only $\sim 0.5\%/^\circ\text{C}$.

The overall field of view is $12.8^\circ \times 6.4^\circ$ in the horizontal and vertical and can be pointed during the flight from horizontal to 10° below the Earth's limb.

The raw signals from each 4×4 SiPM array are routed into a Sensor Interface and Amplifier Board (SIAB), with an integration time of 10 ns. The 32 SIABs receive power and communication through the backplane. On a SIAB, two Multipurpose Integrated Circuit (MUSIC) chips shape and amplify the SiPM signals. The MUSIC chip is an 8-channel, low-power ASIC designed explicitly for SiPM applications in Cherenkov telescopes [49], which monitors the current output of each SiPM channel which is in turn digitized with a 24-bit Analog to Digital Converter (ADC). The temperature of the SiPMs is controlled with a thermistor mounted to the back of each SiPM array and will be used to offline correct temperature-dependent gain drifts of the SiPMs.

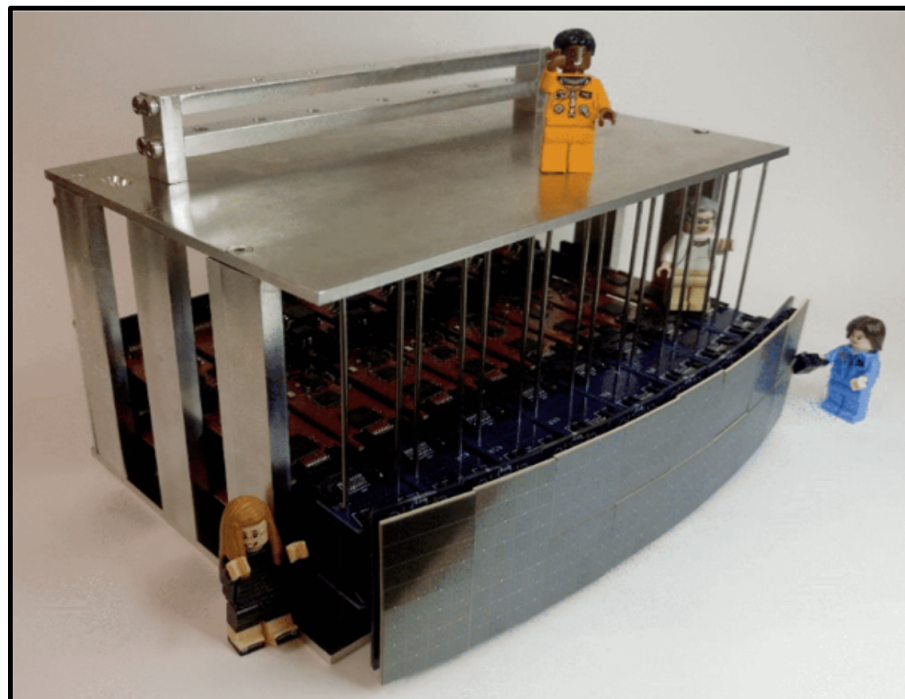


Figure 8. Half assembled Cherenkov camera of EUSO-SPB2 (Lego figures for scale). Image taken from Ref. [41].

The readout of the SiPMs is initiated whenever the bi-focal trigger condition is met [41]. As 90% of the light from a point source at infinity is contained in a 3 mm diameter circle on the focal surface, a typical EAS induced by an Earth-skimming tau-neutrino would usually produce a Cherenkov signal that illuminates only one pixel in the camera. With the bi-focal optics, the Cherenkov signal will be imaged into two pixels separated by one pixel. In Figure 9, the comparison between a simulated EAS (top) and an accidental-triggered event is shown.

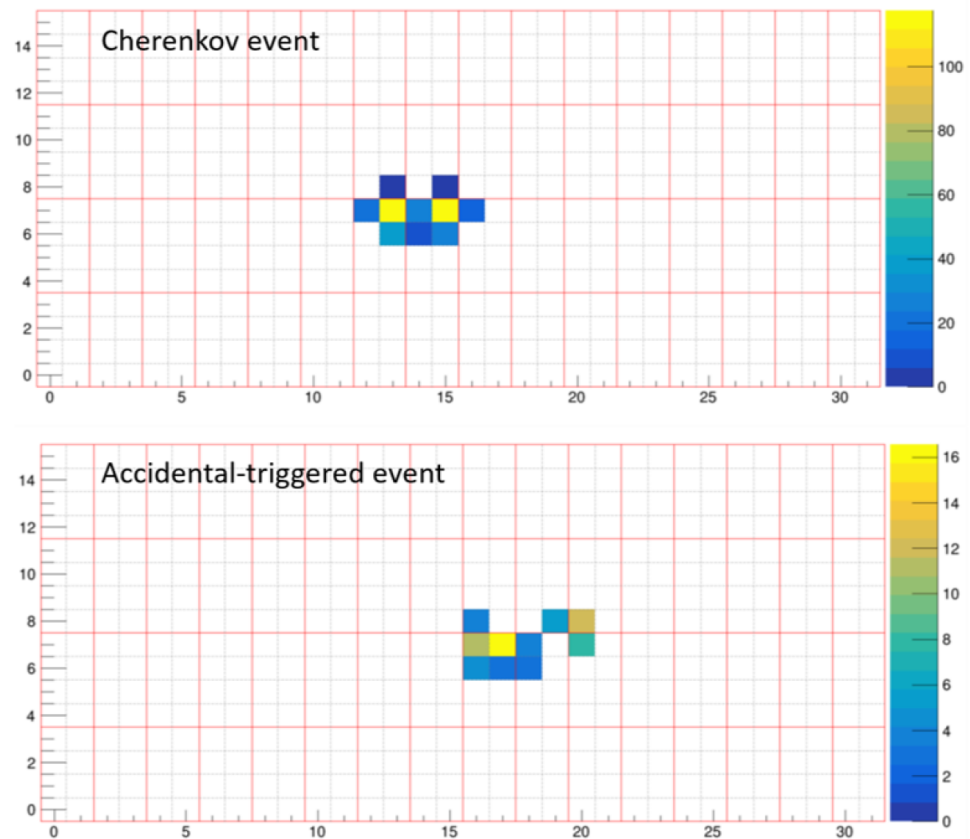


Figure 9. Camera event display of a simulated air-shower event (top) and accidental-triggered event (bottom). Values on the x and y axes are for pixels, and on the color scale are for counts. Image taken from Ref. [41].

The signals from all the 512 SiPM channels are saved in packets of 512 data frames (5.12 μ s long, as the integration time of one frame is 10 ns) centered around the trigger, allowing to target very fast and bright signals such as the Cherenkov emission from EASs. The total power consumption of the Cherenkov telescope is estimated to be about 180 W during operation.

Information regarding the commissioning, calibration, and performance of the CT can be found in Ref. [46]. Throughout the flight, the CT conducted observations over 2 nights, recording approximately 30,000 candidate events, excluding events that did not meet the bifocal condition. The analysis of these events is currently ongoing. Multiple trigger scans were conducted to characterize the background trigger rate when observing both above and below the horizon. The CT was the first to attempt the observation of Cherenkov light from a suborbital altitude, and information about background light and expected trigger rates, including accidentals and actual events, was limited. As of the present writing, data obtained from these scans are still being analyzed to determine the actual rates for both accidentals and candidate events.

3.4. Mini-EUSO (Ancillary Sensors and Day/Night Transition)

The Multiwavelength Imaging New Instrument for the Extreme Universe Space Observatory (Mini-EUSO) [12,50] is the first telescope of the JEM-EUSO Program observing the Earth from space, onboard the ISS, through a nadir-facing UV-transparent window in the Russian Zvezda module. Mini-EUSO is capable of observing EASs generated by UHECRs with an energy above 10^{21} eV and detecting artificial showers generated with lasers from the ground. Other main scientific objectives of the mission are the search for nuclearites and strange quark matter, the study of atmospheric phenomena such as transient luminous events, meteors, and meteoroids, the observation of sea bioluminescence, and of artificial satellites and space debris. It is also mapping the nighttime UV emissions from the Earth, to study the background for the detection of the phenomena described before. The instrument was launched on 22 August 2019, from the Baikonur Cosmodrome and operates a few nights of data taking per month since October 2019. In Figure 10 Mini-EUSO is visible in the hands of a cosmonaut that operated it (Figure 10, left) and once connected to the UV-transparent window of the Zvezda module (Figure 10, right).



Figure 10. Pictures of Mini-EUSO onboard the ISS. Mini-EUSO in the hand of a cosmonaut (left) and connected to the UV-transparent window of the Zvezda module (right). Images taken from Ref. [12] (© AAS. Reproduced with permission).

It is based on an optical system employing two Fresnel lenses of 25 cm diameter and a main focal surface composed of a PDM with MAPMTs. The overall field of view is $44^\circ \times 44^\circ$.

The detector saves triggered transient phenomena with a sampling rate of $2.5 \mu\text{s}$ and 320 ms, as well as continuous acquisition at 40.96 ms scale. The $2.5 \mu\text{s}$ resolution is the highest resolution of Mini-EUSO, also called D1-GTU. Every D1-GTU data are read by the 36 ASICs (1 per MAPMT) and sent to the PDM FPGA board for acquisition and processing. Data are stored by the FPGA in a circular buffer of 128 GTUs. When the trigger conditions are met, 128 data frames centered at the trigger are stored. The trigger algorithm, described in Ref. [51], looks for fluctuations above the average value (dynamically updated) in each pixel. The excess signal must persist for more than 8 D1-GTU ($20 \mu\text{s}$) in any given pixel. The lens size limits the energy threshold to particles above 10^{21} eV, which so far have not been observed. The algorithm worked correctly, triggering on-ground Xenon flashers [52] and ELVES [53]. The 320 μs time resolution (D2-GTU) corresponds to the sum of 128 D1-GTUs and is calculated by the PDM acquisition board. If the trigger conditions are met, data are stored in a similar manner to D1-GTU. The 40.96 ms time resolution (D3-GTU) corresponds to the sum of $128 \times 128 = 16,384$ D1-GTUs and is calculated by the PDM acquisition board. Data frames are saved continuously without a trigger system, to perform a continuous monitoring of the UV emission of the Earth. It is used for the observation of meteors [54],

the search for Strange Quark Matter [55], and for mapping of the night-time terrestrial UV emissions [50].

At the corners of the aperture plane, Mini-EUSO houses two cameras, one in the near-infrared (NIR; 1500–1600 nm) and one in the visible (VIS; 400–780 nm) band, to provide additional information in different frequency ranges. Data are acquired independently of the PDM [56] in 4 s exposure frames.

At the focal surface, next to the PDM, there are a few ancillary cameras, some of them with SiPMs, and are better discussed in the next section.

Ancillary Sensors and Day/Night Transition

As Mini-EUSO is designed to operate at nighttime, the CPU handles cycling between day and night based on the measurements performed by the UV sensors located in the same focal plane of the PDM. It hosts a single-pixel SiPM (Hamamatsu C13365) and two UV photodiodes (Analog Devices AD8304ARUZ with logarithmic response in the range 190–1000 nm, Lapis Semiconductor ML8511 with linear response in the wavelength range 280–400 nm), as visible at the bottom of Figure 11. They are used for information on the day/night transition. The ML8511 UV sensor is normally used for this purpose, although, all three sensors can be used. The photodiode with a linear response is less sensitive than the others, while the SiPM is very sensitive and gets saturated right away. Having multiple ancillary sensors allows us to measure in different illumination conditions. Moreover, they also serve for redundancy, in case one of them (or the electronics) breaks down.



Figure 11. The Mini-EUSO focal surface. The main camera is the PDM with 36 MAPMTs. On top of the PDM there is a 64-channel SiPM array, at the bottom of the PDM there are two UV-light sensors and a single-pixel SiPM. Image adapted from Ref. [12] (© AAS. Reproduced with permission).

Figure 12 shows the light measured by the ML8511 UV sensor as a function of time during a session of data taking. It is possible to see the transition between day and night every ~ 45 min (about half the period of an ISS orbit around the Earth). To avoid fluctuations at the day/night terminator line, 2 thresholds are used to determine the transition from day to night: 60 ADC (Analog to Digital Conversion) counts (blue line); and 100 ADC counts (orange line) from night to day.

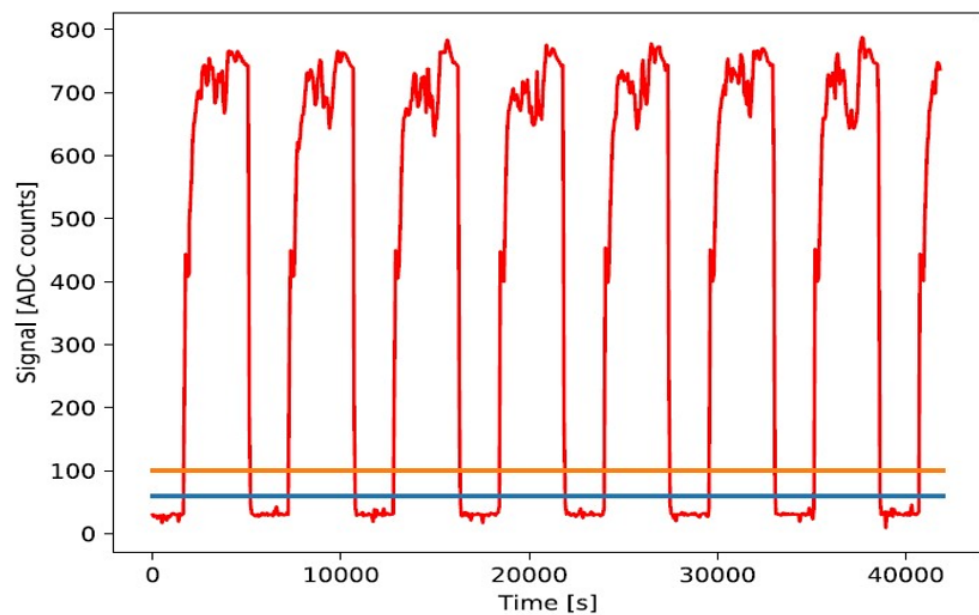


Figure 12. Measurements of the ML8511 UV sensor as a function of time. Mini-EUSO operates at nighttime when the sensor measures a value below 60 ADC counts. To avoid fluctuations at the day–night terminator line, 2 thresholds are used to determine the transition from day to night (60 ADC counts, blue line) and vice-versa (100 ADC counts, orange line). Image taken from [12] (© AAS. Reproduced with permission).

Mini-EUSO also includes a 64-channel SiPM array (Hamamatsu C14047-3050EA08) read independently of the PDM with a multiplexer. The goal of this camera is to test the SiPM array in space.

4. Conclusions

Several experiments of the JEM-EUSO program hosted and host SiPMs: EUSO-SPB1 with the fluorescence camera SiECA; EUSO-SPB2 with the focal surface of the Cherenkov Telescope; Mini-EUSO with the SiPM array and the single-pixel SiPM to evaluate day/night transition. The experience acquired over time was essential for the following experiments, in terms of interfacing them with the other apparatus made with MAPMTs, and in terms of development of the electronics necessary for their operation.

5. Future Directions

At the time of writing, it is foreseen to build in the near future the successor of EUSO-SPB2, called “POEMMA-Balloon with Radio” (or PBR). It will be a telescope with a double focal surface for the observation of the fluorescence and Cherenkov emissions, tiltable from 0° to 90° . It will host auxiliary detectors for the detection of strange quark matter and cameras sensitive to different wavelength ranges: IR, radio, gamma-ray, and X-ray.

For this purpose, there are several activities going on concerning SiPMs, such as the characterization of a few models of SiPMs and the development of the ASIC boards for the Cherenkov cameras. For the development of the gamma-ray detector for the detection, for example, of atmospheric events such as the terrestrial gamma flashers, some designs are under study to discriminate between gamma-rays and charged particles, using SiPMs as sensors.

All the effort is made to obtain stable and reliable detectors in view of future space-based experiments, like POEMMA.

Funding: This research was funded by Basic Science Interdisciplinary Research Projects of RIKEN and JSPS KAKENHI Grant (22340063, 23340081, and 24244042), by the ASI-INAF agreement n.2017-14-H.O, by the Italian Ministry of Foreign Affairs and International Cooperation, by the Italian Space Agency through the ASI INFN agreements Mini-EUSO n. 2016-1-U.0, EUSO-SPB1 n. 2017-8-H.0, OBP n. 2020-26-Hh.0, and EUSO-SPB2 n. 2021-8-HH.0, by NASA award 11-APRA-0058, 16-APROBES16-0023, 17-APRA17-0066, NNX17AJ82G, NNX13AH54G, 80NSSC18K0246, 80NSSC18K0473, 80NSSC19K0626, 80NSSC19K0627, 80NSSC18K0464 and 80NSSC22K1488 in the USA, by the French space agency CNES, by the Deutsches Zentrum für Luft- und Raumfahrt, the Helmholtz Alliance for Astroparticle Physics funded by the Initiative and Networking Fund of the Helmholtz Association (Germany), by Deutsche Forschungsgemeinschaft (DFG, German Research Foundation) under Germany Excellence Strategy—EXC-2094-390783311, by Slovak Academy of Sciences MVTS JEM—EUSO, by National Science Centre in Poland grants 2017/27/B/ST9/02162, 2020/37/B/ST9/01821, and 2022/45/B/ST2/02889 the Polish National Agency for Academic Exchange within Polish Returns Programme no. PPN/PPO/2020/1/00024/U/00001, by Mexican funding agencies PAPIIT-UNAM, CONACyT and the Mexican Space Agency (AEM), as well as VEGA grant agency project 2/0132/17, by grant S2018/NMT-4291 (TEC2SPACE-CM) “Desarrollo y explotación de nuevas tecnologías para instrumentación espacial en la Comunidad de Madrid”, and by State Space Corporation ROSCOSMOS and the Interdisciplinary Scientific and Educational School of Moscow University “Fundamental and Applied Space Research”.

Data Availability Statement: No new data were created or analyzed in this study. The data presented in this study are available in this article.

Conflicts of Interest: The author declares no conflict of interest. The funders had no role in the design of the study; in the collection, analyses, or interpretation of data; in the writing of the manuscript; or in the decision to publish the results.

Abbreviations

The following abbreviations are used in this manuscript:

ADC	Analog to Digital Converter
CMB	Cosmic Microwave Background
CT	Cherenkov Telescope (of EUSO-SPB2)
CTA	Cherenkov Telescope Array
redDCR	redDark Count Rate
EAS	Extensive Air Shower
EC	Elementary Cell
EUSO-SPB1	Extreme Universe Space Observatory on a Super Pressure Balloon (formerly EUSO-SPB)
EUSO-SPB2	Extreme Universe Space Observatory on a Super Pressure Balloon 2
FAMOUS	First Auger Multi-pixel photon counter camera for the Observation of Ultra-high-energy air Showers
FPGA	Field Programmable Gate Array
FT	Fluorescence Telescope (of EUSO-SPB2)
G-APD	Geiger-mode Avalanche Photodiode
GTU	Gate Time Unit
GZK	Greisen–Zatsepin–Kuzmin
IR	Infrared
ISS	International Space Station
JEM-EUSO	Joint Exploratory Missions for an Extreme Universe Space Observatory
MAPMT	Multi-Anode Photo-Multiplier Tubes
Mini-EUSO	Multiwavelength Imaging New Instrument for the Extreme Universe Space Observatory
MPPC	Multi-Pixel Photon Counters
MUSIC	Multipurpose Integrated Circuit
NIR	Near-Infrared
PDE	Photon Detection Efficiency
PDM	Photon-Detection Module
PMMA	Poly(methyl methacrylate)
POEMMA	Probe of Extreme Multi-Messenger Astrophysics

SIAB	Sensor Interface and Amplifier Board
SiECA	Silicon Elementary Cell Add-on
SiPM	Silicon Photomultipliers
SPB	Super Pressure Balloon
TSV	Through Silicon Via
UCIRC	Chicago Infra Red Camera
UHECR	Ultra-High Energy Cosmic Rays
UV	Ultraviolet
VIS	Visible

References

- Renker, D.; Lorenz, E. Advances in solid state photon detectors. *J. Instrum.* **2009**, *4*, P04004. [[CrossRef](#)]
- Acerbi, F.; Gundacker, S. Understanding and simulating SiPMs. *Nucl. Instrum. Methods Phys. Res. A* **2019**, *926*, 16–35. [[CrossRef](#)]
- Gundacker, S.; Heering, A. The silicon photomultiplier: Fundamentals and applications of a modern solid-state photon detector. *Phys. Med. Biol.* **2020**, *65*, 17TR01. [[CrossRef](#)] [[PubMed](#)]
- Nemallapudi, M.V.; Gundacker, S.; Lecoq, P.; Auffray, E. Single photon time resolution of state of the art SiPMs. *J. Instrum.* **2016**, *11*, P10016. [[CrossRef](#)]
- Eckert, P.; Schultz-Coulon, H.C.; Shen, W.; Stamen, R.; Tadday, A. Characterisation Studies of Silicon Photomultipliers. *Nucl. Instrum. Meth.* **2010**, *A620*, 217–226. [[CrossRef](#)]
- Ferri, A.; Acerbi, F.; Gola, A.; Paternoster, G.; Piemonte, C.; Zorzi, N. A comprehensive study of temperature stability of Silicon PhotoMultiplier. *J. Instrum.* **2014**, *9*, P06018. [[CrossRef](#)]
- Parizot, E.; Casolino, M.; Picozza, P.; Ebisuzaki, T.; Bertaina, M.E.; Fuglesang, C.; Haungs, A.; Kajino, F.; Klimov, P.; Olinto, A.; et al. The JEM-EUSO Program for UHECR Studies from Space. *EPJ Web Conf.* **2023**, *283*, 06007. [[CrossRef](#)]
- Abdellaoui, G.; Abe, S.; Adams, J.H., Jr.; Ahriche, A.; Allard, D.; Allen, L.; Alonso, G.; Anchordoqui, L.; Anzalone, A.; Arai, Y.; et al. EUSO-TA—First results from a ground-based EUSO telescope. *Astropart. Phys.* **2018**, *102*, 98–111. [[CrossRef](#)]
- Adams, J.H., Jr.; Ahmad, S.; Allard, D.; Anzalone, A.; Bacholle, S.; Barrillon, P.; Bayer, J.; Bertaina, M.; Bisconti, F.; Blaksley, C.; et al. A Review of the EUSO-Balloon Pathfinder for the JEM-EUSO Program. *Space Sci. Rev.* **2022**, *218*, 3. [[CrossRef](#)]
- Abdellaoui, G.; Abe, S.; Adams, J.H., Jr.; Allard, D.; Alonso, G.; Anchordoqui, L.; Anzalone, A.; Arnone, E.; Asano, K.; Attallah, R.; et al. EUSO-SPB1 Mission and Science. *Astropart. Phys.* **2023**, *154*, 102891. [[CrossRef](#)]
- Eser, J.; Olinto, A.V.; Wiencke, L., for the JEM-EUSO Collaboration. Overview and First Results of EUSO-SPB2. *arXiv* **2023**, arXiv:2308.15693.
- Bacholle, S.; Barrillon, P.; Battisti, M.; Belov, A.; Bertaina, M.; Bisconti, F.; Blaksley, C.; Blin-Bondil, S.; Cafagna, F.; Cambiè, G.; et al. Mini-EUSO mission to study Earth UV emissions on board the ISS. *Astrophys. J. Suppl. Ser.* **2021**, *253*, 2. [[CrossRef](#)]
- Olinto, A.V.; Krizmanic, J.; Adams, J.H.; Aloisio, R.; Anchordoqui, L.A.; Anzalone, A.; Bagheri, M.; Barghini, D.; Battisti, M.; Bergman, D.R. et al. (POEMMA Collaboration). The POEMMA (Probe of Extreme Multi-Messenger Astrophysics) observatory. *J. Cosmol. Astropart. Phys.* **2021**, *2021*, 007.
- Hamamatsu Corporation. *Datasheet 64-Channel MAPMT R11265-00-M64*; Hamamatsu Corporation: Hamamatsu City, Japan, 2009.
- Hamamatsu Corporation. *Datasheet 64-Channel SiPM Array S12642-0808PA-50*; Hamamatsu Corporation: Hamamatsu City, Japan, 2014.
- Schott Corporation. *Datasheet of the BG3 Filter*; Schott Corporation: Mainz, Germany, 2020.
- Bisconti, F. for the JEM-EUSO Collaboration. EUSO-TA fluorescence detector. XXV ECRS 2016 Proceedings—eConf C16-09-04.3. *arXiv* **2016**, arXiv:1701.07091.
- Karus, M. Development of a Calibration Stand for Photosensors for Extremely High-Energy Cosmic Ray Research. Ph.D. Thesis, Karlsruhe Institute of Technology, Karlsruhe, Germany, 2019.
- Ambrosi, G.; Bissaldi, E.; Giglietto, N.; Giordano, F.; Ionica, M.; Paoletti, R.; Rando, R.; Simone, D.; Vagelli, V. for the CTA Consortium. Silicon Photomultipliers and front-end electronics performance for Cherenkov Telescope Array camera development. *Nucl. Instrum. Meth. A* **2017**, *845*, 8–11. [[CrossRef](#)]
- Niggemann, T.; Assis, P.; Brogueira, P.; Bueno, A.; Eichler, H.M.; Ferreira, M.; Hebbeker, T.; Lauscher, M.; Mendes, L.; Middendorf, L.; et al. Status of the Silicon Photomultiplier Telescope FAMOUS for the Fluorescence Detection of UHECRs. In Proceedings of the 33rd International Cosmic Ray Conference (ICRC2013), Rio de Janeiro, Brazil, 2–9 July 2013.
- Tosi, D. for the IceCube-Gen2 Collaboration. Surface detectors for IceCube-Gen2. *J. Instrum.* **2021**, *16*, P08057. [[CrossRef](#)]
- Greisen, K. End to the cosmic-ray spectrum? *Phys. Rev. Lett.* **1966**, *16*, 748. [[CrossRef](#)]
- Zatsepin, G.T.; Kuzmin, V.A. Upper limit of the spectrum of cosmic rays. *Sov. Phys. JETP* **1966**, *4*, 78–80.
- Ave, M.; Bohacova, M.; Buonomo, B.; Busca, N.; Cazon, L.; Chemerisov, S.D.; Conde, M.E.; Crowell, R.A.; Di Carlo, P.; Di Giulio, C. et al. (AIRFLY Collaboration). Spectrally resolved pressure dependence measurements of air fluorescence emission with AIRFLY. *Nucl. Instrum. Methods Phys. Res. Section A* **2008**, *597*, 41–45. [[CrossRef](#)]
- Onsemi Corporation. *Datasheet of C Series SiPMs*; Onsemi Corporation: Scottsdale, AZ, USA, 2014.
- Hamamatsu Corporation. *Datasheet of S13360 Series SiPMs*; Hamamatsu Corporation: Hamamatsu City, Japan, 2021.

27. Hamamatsu Corporation. *Datasheet 64-Channel SiPM Array S13361-3050AS-08*; Hamamatsu Corporation: Hamamatsu City, Japan, 2015.
28. Bisconti, F. Performance of the Cosmic Ray Fluorescence Detector EUSO-TA. Ph.D. Thesis, Karlsruhe Institute of Technology, Karlsruhe, Germany, 2017.
29. Hamamatsu Corporation; New Jersey Institute of Technology. *Low Light Detection: PMT v. SiPM*; Webinar by S. Piatek; Hamamatsu Corporation: Hamamatsu City, Japan, 2016.
30. Onsemi Corporation. *Introduction to the Silicon Photomultiplier (SiPM)*; Application Note; Onsemi Corporation: Scottsdale, AZ, USA, 2011.
31. Bacholle, S., for the JEM-EUSO Collaboration. The EUSO-SPB Instrument. *Proc. Sci.* **2017**, *301*, 384.
32. Adams, J.H., Jr.; Ahmad, S.; Albert, J.N.; Allard, D.; Anchordoqui, L.; Andreev, V.; Anzalone, A.; Arai, Y.; Asano, K.; Ave Pernas, M.; et al. The JEM-EUSO observation in cloudy conditions. *Exp. Astron.* **2015**, *40*, 135. [[CrossRef](#)]
33. Allen, L.; Rezazadeh, M.; Meyer, S.; Olinto, A.V., for the JEM-EUSO Collaboration. UCIRC: Infrared Cloud Monitor for EUSO-SPB1. *Proc. Sci.* **2017**, *301*, 436.
34. Tabone, I.; Bertaina, M.; Carli, D.; Ferrarese, S.; Cremonini, R.; Cassardo, C., for the JEM-EUSO collaboration. The WRF model contribution to the Cloud Top Height retrieval in EUSO-Balloon experiment. *Proc. Sci.* **2015**, *236*, 642.
35. Painter, W. Development of a SiPM Camera for Detection and Measurement of Fluorescence Emission from Extensive Air-Showers Generated by Ultra High Energy Cosmic Rays. Ph.D. Thesis, Karlsruhe Institute of Technology, Karlsruhe, Germany, 2019.
36. Abe, S.; Adams, J.H.; Allard, D.; Alldredge, P.; Anchordoqui, L.; Anzalone, A.; Arnone, E.; Baret, B.; Barghini, D.; Battisti, M.; et al. Developments and results in the context of the JEM-EUSO program obtained with the ESAF Simulation and Analysis Framework. *Eur. Phys. J. C* **2023**, *83*, 1028. [[CrossRef](#)]
37. Haungs, A.; Painter, W.; Bertaina, M.E.; Bortone, A.; Menshikov, A.; Renschler, M., for the JEM-EUSO Collaboration. SiECA: Silicon Photomultiplier Prototype for Flight with EUSO-SPB. *Proc. Sci.* **2017**, *301*, 442.
38. Renschler, M.; Painter, W.; Bisconti, F.; Haungs, A.; Huber, T.; Karus, M.; Schieler, H.; Weindl, A. Characterization of Hamamatsu 64-channel TSV SiPMs. *Nucl. Instrum. Methods Phys. Res. Sect. A* **2018**, *888*, 257–267. [[CrossRef](#)]
39. Kungel, V.; Battisti, M.; Filippatos, G.; Heibges, T.; Kuznetsov, E.; Mese, M.; Meyer, S.S.; Parizot, P.; Scotti, V.; Sternberg, P.; et al., for the JEM-EUSO Collaboration. EUSO-SPB2 Fluorescence Telescope Calibration and Field Tests. *Proc. Sci.* **2023**, *444*, 468.
40. NASA Super Pressure Balloon Mission Terminated Due to Anomaly. Available online: <https://blogs.nasa.gov/superpressureballoon/category/2023-campaign/euso/> (accessed on 1 September 2023).
41. Bagheri, M.; Bertone, P.; Fontane, I.; Gazda, E.; Judd, E.G.; Krizmanic, J.F.; Kuznetsov, E.N.; Miller, M.J.; Nachtman, J.; Onel, Y.; et al., for the JEM-EUSO Collaboration. Overview of Cherenkov Telescope on-board EUSO-SPB2 for the Detection of Very-High-Energy Neutrinos. *Proc. Sci.* **2021**, *395*, 1191.
42. Filippatos, G., for the JEM-EUSO Collaboration. EUSO-SPB2 Fluorescence Telescope in-flight performance and preliminary results. *Proc. Sci.* **2023**, *444*, 251.
43. Blin, S.; Barrillon, P.; de La Taille, C.; Dulucq, F.; Gorodetzky, P.; Prévôt, G., for the JEM-EUSO Collaboration. SPACIROC3: 100 MHz photon counting ASIC for EUSO-SPB. *Nucl. Instrum. Meth. A* **2018**, *912*, 363. [[CrossRef](#)]
44. Filippatos, G.; Battisti, M.; Belov, A.; Bertaina, M.; Bisconti, F.; Eser, J.; Mignone, M.; Sarazin, F.; Wiencke, L. Development of a cosmic ray oriented trigger for the fluorescence telescope on EUSO-SPB2. *Adv. Space Res.* **2022**, *70*, 2794. [[CrossRef](#)]
45. Osteria, G.; Scotti, V.; Peretto, F., for the JEM-EUSO Collaboration. The Data Processor of the EUSO-SPB2 Telescopes. *arXiv* **2023**, arXiv:2310.03012.
46. Romero Matamala, O.F., for the JEM-EUSO Collaboration. Commissioning, Calibration, and Performance of the Cherenkov Telescope on EUSO-SPB2. *Proc. Sci.* **2023**, *444*, 1041.
47. Kungel, V.; Bachman, R.; Brewster, J.; Dawes, M.; Desiato, J.; Eser, J.; Finch, W.; Huelett, L.; Olinto, A.V.; Pace, J. et al., for JEM-EUSO Collaboration. EUSO-SPB2 Telescope Optics and Testing. *Proc. Sci.* **2021**, *395*, 412.
48. Hamamatsu Corporation. *Datasheet 16-Channel SiPM Array S14521-6050AN-04*; Hamamatsu Corporation: Hamamatsu City, Japan, 2018.
49. Gómez, S.; Gascón, D.; Fernández, G.; Sanuy, A.; Mauricio, J.; Graciani, R.; Sanchez D. MUSIC: An 8 channel readout ASIC for SiPM arrays. *Proc. SPIE* **2016**, *9899*. [[CrossRef](#)]
50. Casolino, M.; Barghini, D.; Battisti, M.; Blaksley, C.; Belov, A.; Bertaina, M.; Bianciotto, M.; Bisconti, F.; Blin, S.; Bolmgren, K.; et al. Observation of night-time emissions of the Earth in the near UV range from the International Space Station with Mini-EUSO detector. *Remote Sens. Environ.* **2023**, *284*, 113336. [[CrossRef](#)]
51. Battisti, M.; Barghini, D.; Belov, A.; Bertaina, M.; Bisconti, F.; Bolmgren, K.; Cambiè, G.; Capel, F.; Casolino, M.; Ebisuzaki, T. Onboard performance of the level 1 trigger of the mini-EUSO telescope. *Adv. Space Res.* **2022**, *70*, 2750. [[CrossRef](#)]
52. Battisti, M.; Bertaina, M.; Arnone, E.; Pretto, G.; Sammartino, G., for the JEM-EUSO Collaboration. Analysis of EAS-like events detected by the Mini-EUSO telescope. *Proc. Sci.* **2023**, *444*, 353.
53. Romoli, G., for the JEM-EUSO Collaboration. Study of multiple ring ELVES with the Mini-EUSO telescope on-board the International Space Station. *Proc. Sci.* **2023**, *444*, 223.
54. Barghini, D.; Battisti, M.; Belov, A.; Bertaina, M.E.; Bertone, S.; Bisconti, F.; Capel, F.; Casolino, M.; Cellino, A.; Ebisuzaki, T.; et al. Analysis of meteors observed in the UV by the Mini-EUSO telescope onboard the International Space Station. *Eur. Sci. Congr.* **2021**, *15*, EPSC2021-243.

-
55. Casolino, M., for the JEM-EUSO Collaboration. Search for Strange Quark Matter from the International Space Station with the Mini-EUSO experiment. *Proc. Sci.* **2023**, *444*, 1410.
 56. Turriziani, S.; Kelund, J.; Tsuno, K.; Casolino, M.; Ebisuzaki, T. Secondary cameras onboard the Mini-EUSO experiment: Control Software and Calibration. *Adv. Space Res.* **2019**, *64*, 1188–1198. [[CrossRef](#)]

Disclaimer/Publisher’s Note: The statements, opinions and data contained in all publications are solely those of the individual author(s) and contributor(s) and not of MDPI and/or the editor(s). MDPI and/or the editor(s) disclaim responsibility for any injury to people or property resulting from any ideas, methods, instructions or products referred to in the content.